SCIENTIFIC REPORTS

OPEN

Received: 29 March 2017
Accepted: 4 August 2017
Published online: 25 August 2017

The Parkinson's disease-associated GPR37 receptor interacts with striatal adenosine A_{2A} receptor controlling its cell surface expression and function *in vivo*

Xavier Morató[1,2], Rafael Luján[3], Marc López-Cano[1,2], Jorge Gandía[1,2], Igor Stagljar[4], Masahiko Watanabe[5], Rodrigo A. Cunha[6], Víctor Fernández-Dueñas[1,2] & Francisco Ciruela[1,2]

G protein-coupled receptor 37 (GPR37) is an orphan receptor associated to Parkinson's disease (PD) neuropathology. Here, we identified GPR37 as an inhibitor of adenosine A_{2A} receptor (A_{2A}R) cell surface expression and function *in vivo*. In addition, we showed that GPR37 and A_{2A}R do oligomerize in the striatum. Thus, a close proximity of GPR37 and A_{2A}R at the postsynaptic level of striatal synapses was observed by double-labelling post-embedding immunogold detection. Indeed, the direct receptor-receptor interaction was further substantiated by proximity ligation *in situ* assay. Interestingly, GPR37 deletion promoted striatal A_{2A}R cell surface expression that correlated well with an increased A_{2A}R agonist-mediated cAMP accumulation, both in primary striatal neurons and nerve terminals. Furthermore, GPR37−/− mice showed enhanced A_{2A}R agonist-induced catalepsy and an increased response to A_{2A}R antagonist-mediated locomotor activity. Overall, these results revealed a key role for GPR37 controlling A_{2A}R biology in the striatum, which may be relevant for PD management.

GPR37, also known as parkin-associated endothelin-like receptor (Pael-R), is an orphan G protein-coupled receptor (GPCR) expressed in brain regions such as cerebellum, corpus callosum, caudate nucleus, putamen, substantia nigra and hippocampus[1,2]. The physiological function of this receptor has not been still elucidated. Thus, GPR37 is known to be expressed in neural progenitor cells and control Wnt signaling[3]. Also, a GPR37-mediated control of oligodendrocyte differentiation has been recently described[4], but scarce information exists regarding its presence in other neuronal subsets. On the other hand, the neuropathological role of GPR37 has been extensively studied. Hence, it is well-established that GPR37 is a substrate for parkin, an E3 ubiquitin ligase involved in the ubiquitination and proteasome-mediated degradation/clearance of misfolded proteins[5]. Indeed, both the loss of function of parkin and its toxic accumulation have been found in some states of Parkinson's disease (PD)[6–8]. Of note, it was recently described that GPR37 suffers constitutive metalloproteinase-mediated proteolysis, which results on the release of an N-terminal ectodomain[9]. Accordingly, this ecto-domain could be responsible for its toxicity upon overexpression. Alternatively, a role for GPR37 on neuroprotection has been also suggested, since it has been associated with the action of some peptides[10]. Nevertheless, the toxic effects of GPR37 accumulation seem clear in PD. Thus, GPR37 up-regulation, or the presence of GPR37 in Lewy bodies, has been found in brains from PD patients[11–13]. Furthermore, it was shown that the absence of GPR37 in a mouse model of PD (i.e. MPTP) protected against dopaminergic cell death[14].

[1]Unitat de Farmacologia, Departament Patologia i Terapéutica Experimental, Facultat de Medicina, IDIBELL, Universitat de Barcelona, L'Hospitalet de Llobregat, Barcelona, Spain. [2]Institut de Neurociències, Universitat de Barcelona, Barcelona, Spain. [3]IDINE, Departamento de Ciencias Médicas, Facultad de Medicina, Universidad Castilla-La Mancha, Albacete, Spain. [4]Donnelly Centre, Department of Molecular Genetics, Department of Biochemistry, University of Toronto, Toronto, M5S 3E1, Canada. [5]Department of Anatomy, Hokkaido University School of Medicine, Sapporo, 060-0818, Japan. [6]CNC-Center for Neuroscience and Cell Biology, Faculty of Medicine, University of Coimbra, Coimbra, Portugal. Correspondence and requests for materials should be addressed to V.F.-D. (email: vfernandez@ub.edu) or F.C. (email: fciruela@ub.edu)

The role of GPR37 in PD has been investigated focusing on the interaction of this orphan receptor with different neurotransmitter systems. In such way, it has been shown that GPR37 deletion increases pre-synaptic dopamine transporter (DAT) cell surface expression in the striatum[15]. Similarly, it has been described that the adenosinergic-dependent control of anxiety behavior is modified in GPR37 deficient mice (GPR37−/−)[2], and that upon deletion of GPR37, adenosine A_{2A} receptors ($A_{2A}R$) antagonists cannot revert pilocarpine-induced tremor, which is a model for parkinsonism[16]. On the other hand, some data point to the existence of direct receptor-receptor interactions involving GPR37. Thus, it was firstly proposed that GPR37 may interact with dopamine D_2 receptors (D_2R)[17]. Indeed, it has been recently hypothesized that GPR37 and $A_{2A}R$ might form receptor-receptor complexes or heteromers in the striatum[18], a fact that has not been still wholly demonstrated. Interestingly, the existence of a direct receptor-receptor interaction between $A_{2A}R$ and dopamine D_2 receptor (D_2R) in the striatum was recently demonstrated and proposed as a pharmacological target for PD management[19]. Hence, it could be postulated that the relevance of GPR37 in PD could be related to its interaction with striatal $A_{2A}R$ and/or D_2R. Supporting this idea, we recently reported that GPR37−/− mice showed lower haloperidol-induced catalepsy[18], thus suggesting an altered functioning of postsynaptic striatal D_2R[20] in GPR37−/− mice. In addition, the well-known effects of $A_{2A}R$ antagonists blocking haloperidol-induced catalepsy were higher in the absence of GPR37, thus suggesting a GPR37-dependent $A_{2A}R$ modulation of dopaminergic transmission. Overall, GPR37 may play a key role in the $A_{2A}R$-D_2R interplay and consequently it could be considered as a novel target for PD management.

Here, we aimed to validate the existence of GPR37-$A_{2A}R$ oligomers in the striatum and to assess the functional impact of this receptor-receptor interaction *in vivo*. Accordingly, we examined the effects of GPR37 presence/absence on $A_{2A}R$ localization (cell surface targeting) and function (cAMP accumulation and behavioral activities, namely catalepsy and locomotor activity).

Results

Striatal GPR37 and $A_{2A}R$ are enriched at the postsynaptic compartment. By using a systematic interactome mapping of protein-protein interactions for the $A_{2A}R$, we recently identified and validated GPR37 receptor as a putative interacting partner of $A_{2A}R$[18]. Here, we first aimed to wholly demonstrate and characterize the existence of this direct receptor-receptor interaction (i.e. GPR37-$A_{2A}R$ oligomerization) in native tissue. To this end, we first determined the regional and overlapping localization of these two receptors in the mouse brain by using conventional immunohistoblotting. GPR37 was widely distributed throughout the brain with a high degree of expression in myelinated tracts including *corpus callosum* and cerebellar white matter tracts (Fig. 1A), as previously described by means of *in situ* hybridization[4]. In addition, a moderate to weak labeling was consistently detected in cortex, striatum and hippocampus (Fig. 1A and B). Interestingly, no immunostaining was observed when brain sections from GPR37−/− were used (Fig. 1A), thus demonstrating the specificity of the antibody used (i.e. rabbit anti-GPR37-N). Finally, under the same experimental conditions we found that $A_{2A}R$ expression was mostly concentrated in the striatum (Fig. 1), as expected[21,22]. Overall, these first experiments pinpointed the striatum as a brain region to assess GPR37-$A_{2A}R$ interaction.

Next, we aimed to ascertain the subsynaptic striatal locus where a putative interaction between these two receptors might occur. We first evaluated the subcellular localization of GPR37 within the striatum by means of immunogold electron microscopy. GPR37 immunoparticles were mostly found at the extrasynaptic plasma membrane of dendritic spines of striatal neurons (Fig. 2A, arrows), with few immunoparticles present at intracellular sites (Fig. 2A, crossed arrows). Similarly, in axon terminals establishing asymmetrical synapses with striatal spines GPR37 immunoparticles were also localized at the extrasynaptic plasma membrane (Fig. 2A, lower panel, arrowheads). Finally, in dendritic shafts, immunoparticles for GPR37 were mainly found at the plasma membrane (Fig. 2A, lower panel arrows). Interestingly, quantitative analysis showed that $26 \pm 0.9\%$ of immunoparticles were located presynaptically while $73 \pm 0.9\%$ showed a postsynaptic distribution (Fig. 2B), thus matching with $A_{2A}R$ distribution within the striatum[21]. Subsequently, we performed a subsynaptic fractionation of striatal nerve terminals, which allowed identifying the localization of GPR37 and $A_{2A}R$[23,24] in pre-, post- and extrasynaptic enriched fractions (Fig. 2C). Interestingly, immunoblot analysis of the different striatal subsynaptic fractions revealed a significant ($P < 0.05$) enrichment at the postsynaptic over the presynaptic fraction of both GPR37 and $A_{2A}R$ (Fig. 2C and D), thus showing their superimposable subsynaptic distribution within the striatum. On the other hand, we ascertained the well-characterized high $A_{2A}R$ extrasynaptic expression, which has been reported to be mostly related to the actions of adenosine acting as an energy-dependent neuromodulator in the SNC, also finely sensoring neuronal activity[25].

Co-clustering of GPR37 and $A_{2A}R$ in striatum. While biochemical approaches are useful to establish the subsynaptic distribution of neuronal proteins they do not provide spatial information. Thus, we aimed to determine the proximity between GPR37 and $A_{2A}R$ within striatal neurons by means of double-labelling immunogold electron microscopy and proximity ligation *in situ* assay (P-LISA). First, it was observed that GPR37 and $A_{2A}R$ closely co-distributed along the extrasynaptic plasma membrane of dendritic shafts and dendritic spines establishing excitatory synaptic contact with axon terminals (Fig. 3A–D). This result agrees with the previously findings reported in the subsynaptic fractionation experiments. Importantly, in the striatum of GPR37−/− mice, no GPR37 detection was observed (Fig. 3E), again demonstrating the specificity of the anti-GPR37-N antibody used. Overall, these results revealed a close and selective anatomical proximity of GPR37 and $A_{2A}R$ within striatal spines.

We next aimed to validate the existence of GPR37/$A_{2A}R$ heteromers in the striatum by means of P-LISA, a well described technique that provides enough sensitivity to evaluate receptor's close proximity within a named GPCR oligomer in native conditions[26]. We first ascertained the immunohistochemistry detection of GPR37 and $A_{2A}R$ in the striatum. As expected, both receptors showed a high degree of co-distribution throughout the striatal

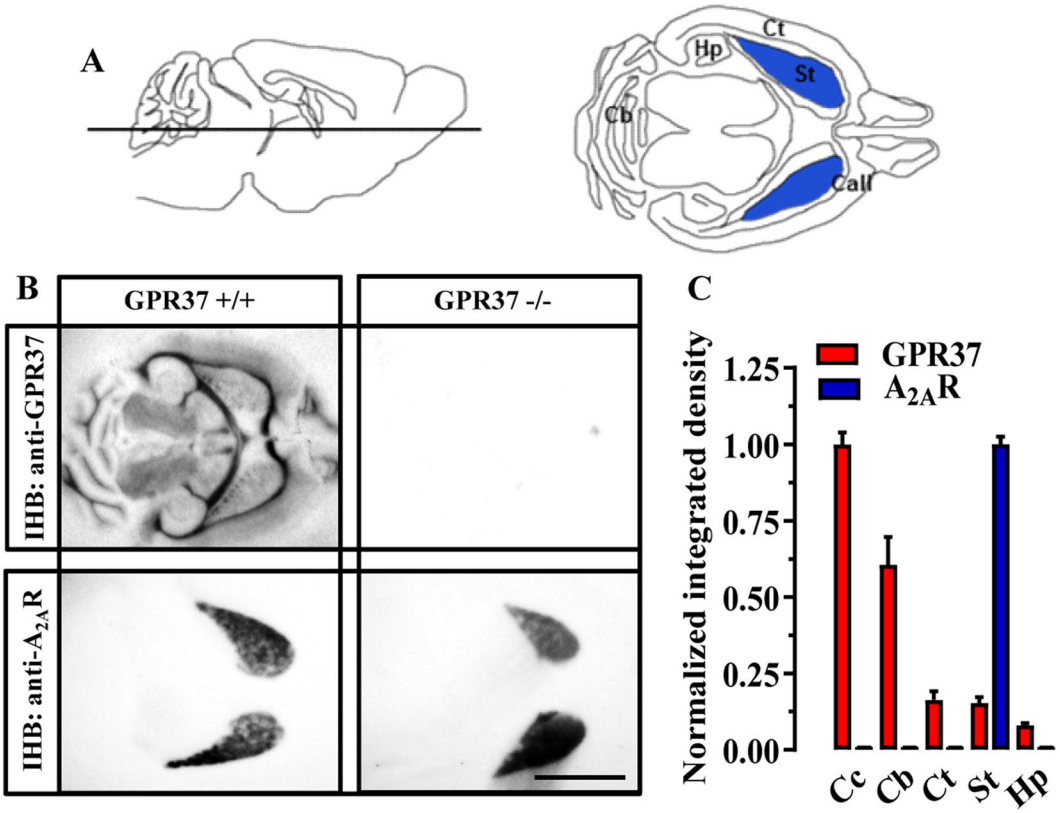

Figure 1. Co-distribution of GPR37 and $A_{2A}R$ in the mouse brain. (**A**) Cartoon showing the location of the horizontal brain section for the histoblot (left panel). The expected brain regions within the horizontal section (right panel) are indicated: Cb, cerebellum; Hp, hippocampus; Ct, cortex; St, striatum (blue); Call, corpus callosum. (**B**) Histoblots from horizontal sections (see panel A) of GPR37+/+ and GPR37−/− mouse brain. GPR37 and $A_{2A}R$ were detected using a rabbit anti-GPR37-N antibody (3 μg/ml) and a goat anti-$A_{2A}R$ antibody (3 μg/ml) (see Materials and Methods). (**C**) The histoblots were scanned and densitometric measurements from six independent experiments were averaged to compare the GPR37 and $A_{2A}R$ protein densities. Since expression was maximal in *corpus callosum*, normalization was performed assigning it the 100%. Results are expressed as mean ± SEM. Scale bar: 0.4 cm.

neuropil (Fig. 4A). Interestingly, no immunostaining was observed when brain slices from GPR37−/− were used (Fig. 1A, upper right panel), thus demonstrating the specificity of the antibody used (i.e. rabbit anti-GPR37-C). Noteworthy, here we used an antibody directed against the C-terminus of GPR37. This is a mandatory requirement for the PLA assay, in which both antibodies must recognize the extracellular or intracellular epitopes of the selected putative interacting proteins. Subsequently, we implemented the P-LISA approach, using an adequate combination of antibodies to test the presence of GPR37/$A_{2A}R$ heteromers in the mouse striatum. Notably, red dots reflecting a positive P-LISA signal were observed in the striatum of GPR37+/+ mice (Fig. 4B, upper panel), thus allowing the visualization of the GPR37/$A_{2A}R$ receptor-receptor interaction. Importantly, in striatal slices from GPR37−/− mice the P-LISA signal was negligible (Fig. 4B, lower panel), thus reinforcing the specificity of our P-LISA assay. Indeed, when the P-LISA signal was quantified, 6.5 ± 1.6 dots/nuclei were observed in GPR37+/+ mice, while GPR37−/− mice only displayed 0.9 ± 0.3 dots/nuclei under the same experimental conditions. Thus, a marked and significant ($P < 0.05$) reduction in the P-LISA signal was observed in GPR37−/− striatal slices, which strongly supported the existence of GPR37/$A_{2A}R$ heteromers in the mouse striatum.

GPR37 deletion promotes striatal $A_{2A}R$ cell surface expression and function. It has been shown that GPR37 cell surface expression in cultured cells can be regulated by co-expressing particular GPCRs, including the $A_{2A}R$[17]. Indeed, we recently demonstrated that GPR37 and $A_{2A}R$ form heteromers *in vitro* with an intertwined cell surface expression when co-expressed[18]. However, the function of the GPR37-$A_{2A}R$ interaction in native tissue is still enigmatic. Therefore, we aimed to ascertain the impact of GPR37 expression on $A_{2A}R$ trafficking and function in native tissues. To this end, we first assessed $A_{2A}R$ cell surface expression by means of biotynilation of striatal slices, thus enabling the selective quantification of surface expressed receptors in GPR37+/+ and GPR37−/− mice. Interestingly, while total $A_{2A}R$ density was unaltered, the $A_{2A}R$ cell surface density was increased in the striatum of GPR37−/− mice (Fig. 5A and B). Of note, the absence of tyrosine hydroxylase immunoreactivity in the biotinylated surface fractions indicated that the integrity of slices was maintained and no major cell damage occurred during striatal slice preparation. Thus, our results demonstrated that GPR37 deletion potentiates $A_{2A}R$ cell surface expression.

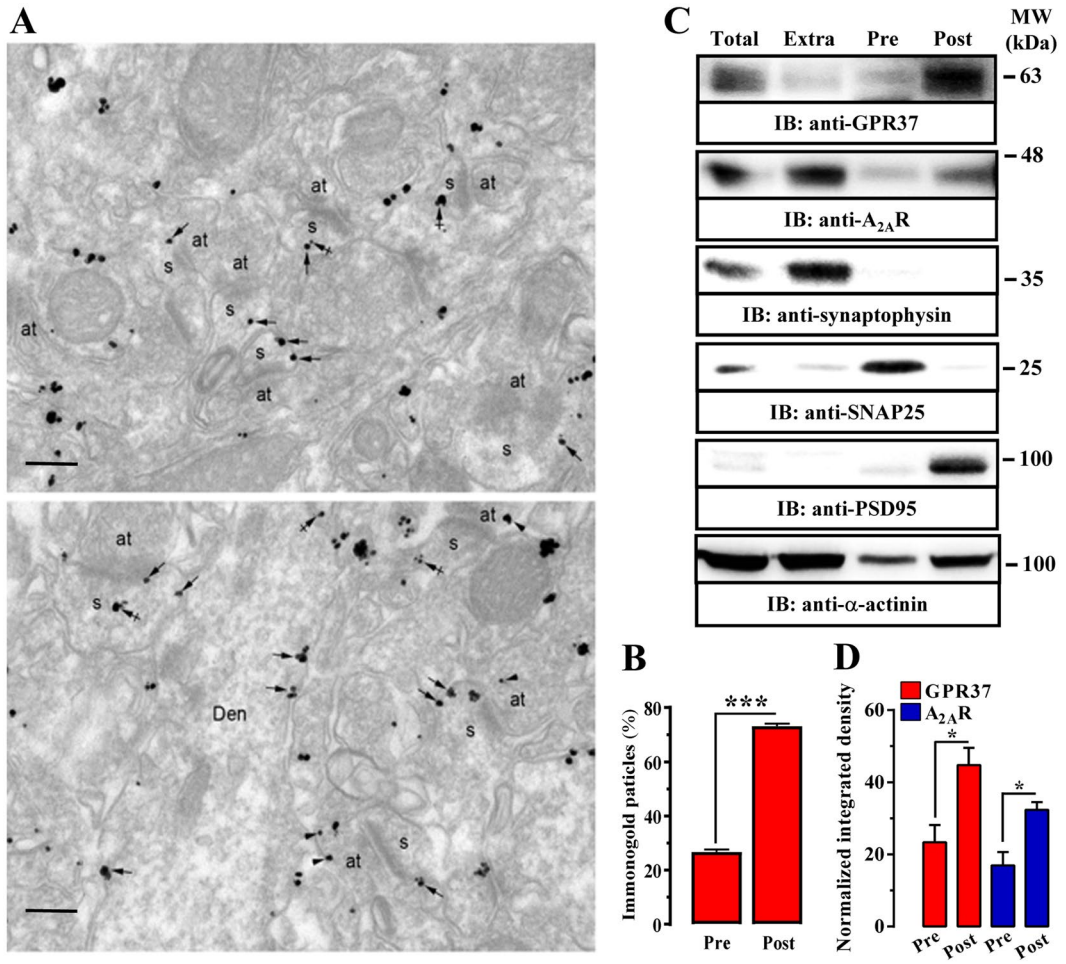

Figure 2. Subsynaptic distribution of GPR37 in the mouse striatum. (**A**) Electron micrographs showing immunoparticles for GPR37 in the striatum of GPR37+/+ mice using the pre-embedding immunogold technique. GPR37 immunoparticles were abundant on the extrasynaptic plasma membrane (arrows) of dendritic spines (s) of striatal neurons contacted by axon terminals (at). Few immunoparticles were observed at intracellular sites (crossed arrows) in dendritic spines (s) (upper panel). Immunoparticles for GPR37 were also localized to the extrasynaptic plasma membrane (arrowheads) of axon terminals (at) establishing asymmetrical synapses with spines (s). In dendritic shafts (Den), immunoparticles for GPR37 were mainly found at the plasma membrane (arrows) (lower panel). Scale bars: 200 nm. (**B**) Bar graphs showing the percentage of GPR37 immunoparticles at post- and presynaptic compartments. The data are expressed as mean ± SEM of three independent experiments (***$P < 0.001$; Student's *t*-test). (**C**) Representative immunoblots showing GPR37 and $A_{2A}R$ immunoreactivity in striatal synaptic fractions. Striatal synaptosomes (Total) were subcellularly fractionated (see Materials and Methods section) into extrasynaptic (Extra), presynaptic active zone (Pre) and postsynaptic density (Post) fractions, which were analyzed by SDS-PAGE (20 μg of protein/lane) and immunoblotted using rabbit anti-GPR37-N, goat anti-$A_{2A}R$, rabbit anti-synaptophysin, mouse anti-PSD-95, mouse anti-SNAP-25 and rabbit anti-α-actinin antibodies. The primary antibodies were detected using a horseradish peroxidase (HRP)-conjugated goat anti-rabbit IgG, HRP-conjugated goat anti-mouse IgG, HRP-conjugated rabbit anti-goat IgG and chemiluminescence detection (see Materials and Methods). (**D**) Relative quantification of GPR37 enrichment in striatal presynaptic and postsynaptic fractions. The intensities of the immunoreactive bands on the immunoblotted membranes corresponding to extrasynaptic, presynaptic (Pre) and postsynaptic (Post) fractions were measured by densitometric scanning. Values were first normalized to the loading control (i.e. α-actinin) and then to the amount of GPR37 or $A_{2A}R$ in the total fraction. Data are expressed as mean ± SEM of three independent experiments (*$P < 0.05$, Student's *t*-test).

Next, we examined whether the increased $A_{2A}R$ cell surface expression in GPR37−/− striatum translated into an increased $A_{2A}R$ function. To this end, we evaluated $A_{2A}R$-dependent cAMP accumulation in striatal nerve terminals from GPR37+/+ and GPR37−/− mice. First, we undertook a complementary double immunocytochemistry study in individual striatal synaptosomes to identify synapses endowed with both GPR37 and $A_{2A}R$ (Fig. 5C). As illustrated in Fig. 5D, we observed that around 9 ± 1.1% of total population of striatal synaptosomes (immunopositive for both SNAP25 and PSD95), presented immunoreactivity for both GPR37 and $A_{2A}R$ (Fig. 5D). Subsequently, we compared the ability of an $A_{2A}R$ agonist to trigger cAMP accumulation in striatal

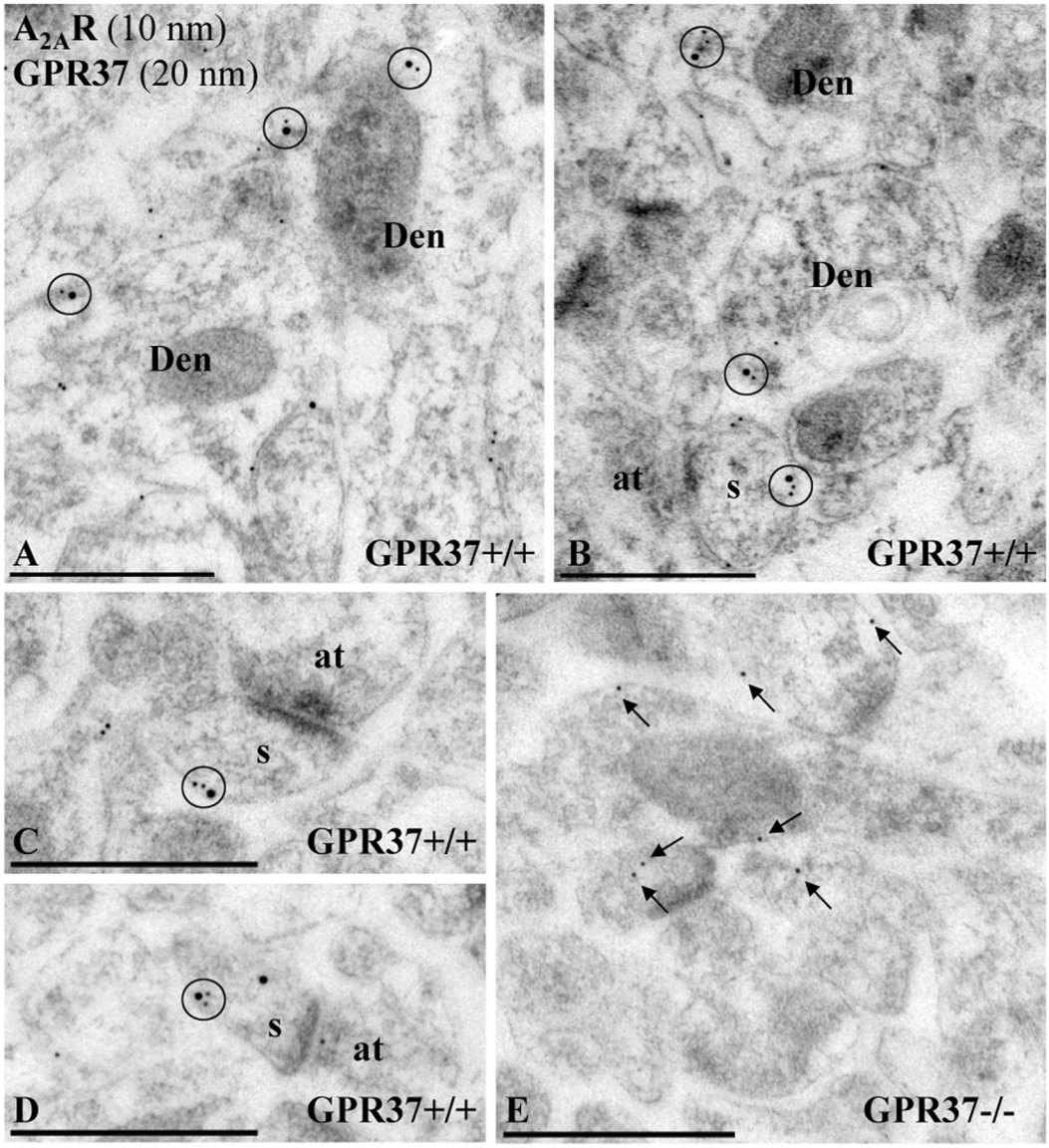

Figure 3. Post-embedding electron microscopy showing GPR37 and $A_{2A}R$ co-localization in the mouse striatum. Electron micrographs from GPR37+/+ and GPR37−/− showing immunoreactivity for GPR37 and $A_{2A}R$ in the striatum revealed using a double-labelling post-embedding immunogold technique. (**A–D**) In GPR37+/+ mice, immunoparticles for $A_{2A}R$ (10 nm size) and GPR37 (20 nm size) were closely co-distributed (circles) along the extrasynaptic plasma membrane of dendritic shafts (Den) and dendritic spine (s) establishing excitatory synaptic contact with axon terminals (b). (**E**) In GPR37−/− mice, immunoparticles for $A_{2A}R$ (10 nm size) are present in the tissue but not immunoparticles for GPR37, demonstrating the full specificity of the anti-GPR37-N antibody. Scale bars: A–E, 500 nm.

synaptosomes from GPR37+/+ and GPR37−/− mice. A significant 2.5-fold increase in $A_{2A}R$-mediated cAMP accumulation was observed in synaptosomes from GPR37−/− mice (Fig. 5E). Finally, similar $A_{2A}R$-based functional assays were performed in striatal primary neurons from GPR37+/+ and GPR37−/− mice (Fig. 5F). Again, a significant increase in $A_{2A}R$-mediated cAMP accumulation was observed in primary cultures from GPR37−/− striatum (Fig. 5G). Overall, these results demonstrated that GPR37 deletion bolstered striatal $A_{2A}R$ cell surface expression as well as $A_{2A}R$ function.

GPR37 deletion enhances $A_{2A}R$ function *in vivo*. Once we confirmed an enhanced striatal $A_{2A}R$ activity in GPR37−/− mice, we aimed to determine its impact in animal behavior. It is well established that striatal $A_{2A}R$ modulates the central processes involved in locomotor activity and psychomotor behaviors due to its interplay with the dopaminergic system[27]. Our data predicted an enhanced modulation of locomotor activity by striatal $A_{2A}R$ in GPR37−/− mice. Since it is well-known that blocking of $A_{2A}R$ increases spontaneous locomotor activity in mice[28], we compared the hyper-motility induced by an $A_{2A}R$ antagonist in GPR37+/+ and GPR37−/− mice. To this end, we challenged GPR37+/+ and GPR37−/− mice with SCH58261 and the spontaneous locomotor

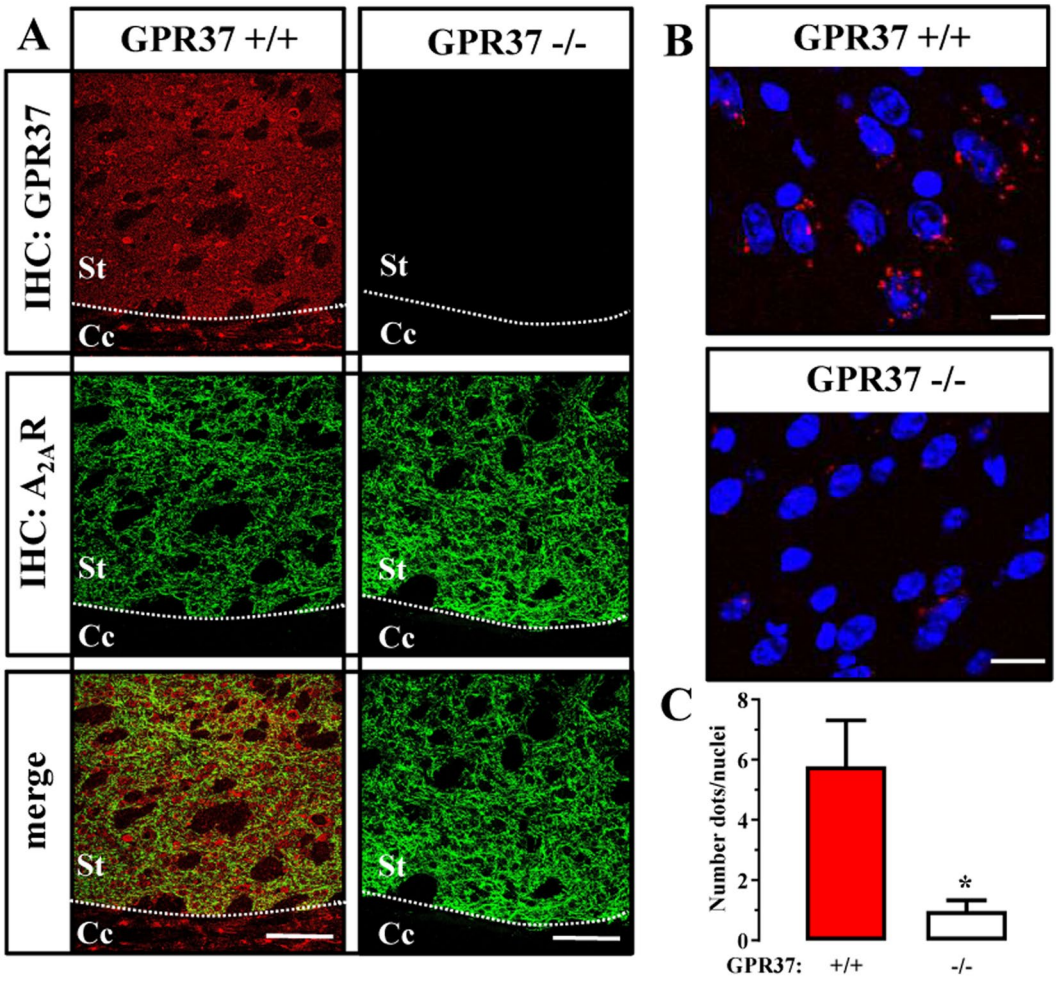

Figure 4. GPR37 and $A_{2A}R$ interact in the striatum. (**A**) Representative images of GPR37 and $A_{2A}R$ immunoreactivities in the dorsal striatum of GPR37+/+ and GPR37−/− mice. Superimposition of images revealed receptor co-distribution in yellow (merge). Scale bar: 350 μm. Cc, corpus callossum; St; striatum. (**B**) Photomicrographs of dual recognition of GPR37 and $A_{2A}R$ with P-LISA in striatal sections from GPR37+/+ and GPR37−/− mice. Scale bar: 10 μm. (**C**) Quantification of P-LISA signals for GPR37 and $A_{2A}R$ proximity in GPR37+/+ and GPR37−/−. Values in the graph correspond to the mean ± SEM (dots/nuclei) of at least five animals for each condition. Asterisk indicates statistically significant differences ($p < 0.05$; Student's *t*-test) when comparing GPR37−/− with GPR37+/+.

activity in an open field arena was monitored (Fig. 6A). Our results showed that $A_{2A}R$ antagonist-mediated locomotor activity potentiation was significantly ($P < 0.05$) higher in GPR37−/− mice (Fig. 6B), thus suggesting an increased $A_{2A}R$ basal activity in the absence of GPR37.

Conversely to hyperlocomotion induced by $A_{2A}R$ antagonists, activation of striatal $A_{2A}R$ with selective agonists can suppress motor activity, thus producing effects that resemble those yielded by D_2R antagonists (i.e. haloperidol) or dopamine depletion (i.e. reserpine)[29]. For instance, administration of the $A_{2A}R$ agonist CGS 21680 blocked acquisition and expression of wheel running behavior[30], depressed locomotor activity[31] and induced catalepsy[32]. We now assessed whether $A_{2A}R$ agonist-induced catalepsy was increased in GPR37−/− mice. Our results showed that upon CGS21680 administration (i.c.v.) the catalepsy scores of GPR37−/− mice were significantly higher ($P < 0.001$) than these observed in GPR37+/+ mice (Fig. 6C), thus demonstrating an increased activity of striatal $A_{2A}R$ in GPR37−/− mice. Overall, our results suggested that GPR37 may modulate $A_{2A}R$ control of locomotor activity and psychomotor behavior through a putative GPR37/$A_{2A}R$ heteromer. Needless to say, as commented previously, GPCR display the ability to oligomerize, but receptors may also exist in their monomeric form. Accordingly, the observed effects of $A_{2A}R$ ligands on locomotor activity and psychomotor activity would be interpreted within this more complex scenario, in which different populations of receptors exist, forming or not heteromers.

Discussion

GPR37 is an orphan GPCR highly expressed throughout the brain. Although it has been related to the dopaminergic system[15] and brain myelination[4], the physiological role of this receptor has not been fully elucidated.

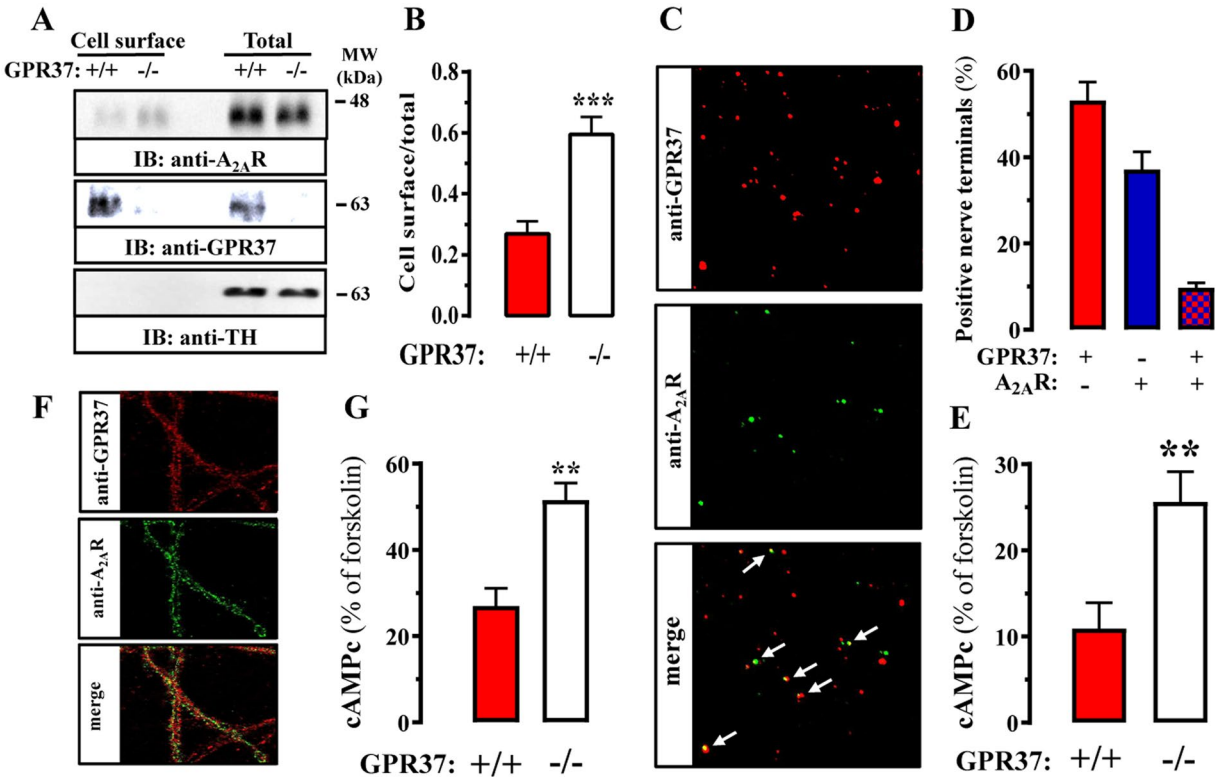

Figure 5. GPR37 deletion bolsters striatal $A_{2A}R$ cell surface expression and function. (**A**) Coronal brain slices (300 µm) from GPR37+/+ and GPR37−/− mice were prepared and biotinylated as described in Material and Methods section. Total and cell surface extracts were analyzed by SDS-PAGE and immunoblotting as described in Fig. 2. (**B**) Quantification of $A_{2A}R$ cell surface density in GPR37+/+ and GPR37−/− striatum. Cell surface density was normalized using the total density of $A_{2A}R$ and expressed as mean ± SEM from six independent experiments. The asterisk indicates statistically significant difference from the control condition ($P < 0.05$; paired Student's *t* test). (**C**) Co-distribution of GPR37 and $A_{2A}R$ in striatal synaptosomes. Immunofluorescence detection of GPR37 (red) and $A_{2A}R$ (green) in striatal total synaptosomes was performed as described in Materials and Methods. Superimposition of images (merge) reveals co-localization in yellow (arrows). (**D**) Quantification of synaptosomes expressing GPR37 and/or $A_{2A}R$. The data are expressed as the percentage (mean ± SEM) of total number of synaptosomes that are endowed with GPR37 and/or $A_{2A}R$, quantified in 3–4 different synaptosomal preparations from different mice, in which four different fields acquired from two different coverslips were analysed in each preparation. (**E**) $A_{2A}R$-mediated cAMP accumulation in synaptosomes. Total striatal synaptosomes from GPR37+/+ and GPR37−/− mice were stimulated with 500 nM CGS21680 for 30 min at 37 °C and the cAMP accumulation was measured as described in Materials and Methods. The data are expressed as percentage (mean ± SEM) of forskolin-induced cAMP accumulation from eight independent experiments, which was similar ($P > 0.05$) in both genotypes. The asterisks indicate statistically significant difference from the control condition ($P < 0.01$; Student's *t* test). (**F**) Co-distribution of GPR37 and $A_{2A}R$ in striatal neurons. Immunofluorescence detection of GPR37 (red) and $A_{2A}R$ (green) in primary cultured striatal neurons (DIV21) was performed as described in Materials and Methods. Superimposition of images (merge) reveals co-localization in yellow. Scale bar: 100 µm. (**G**) $A_{2A}R$-mediated cAMP accumulation in striatal neurons. Striatal primary neurons from GPR37+/+ and GPR37−/− were stimulated with 500 nM CGS21680 for 30 min at 37 °C and the cAMP accumulation was measured as described in Materials and Methods. The data are expressed as percentage (mean ± SEM) of forskolin-induced cAMP accumulation from five independent experiments, which was similar ($P > 0.05$) in both genotypes. The asterisks indicate statistically significant difference from the control condition ($P < 0.01$; Student's *t* test).

Recently, by using a modified membrane yeast two-hybrid (MYTH) approach, GPR37 was identified as a putative $A_{2A}R$ interacting partner[18], prompting the exploration of the biological relevance of this interaction in the native brain. Our experimental data strongly supports the existence of GPR37/$A_{2A}R$ heteromers in the mouse striatum. Thus, the former GPR37-$A_{2A}R$ interaction picked up *in vitro* by MYTH[18] was further validated in native tissue by double-labelling immunogold electron microscopy and P-LISA, which permitted to definitely establish the existence of a close proximity between these two receptors in the mouse striatum. These findings prompted us to assess the impact of this oligomer in animal behavior. Accordingly, our main objective consisted of unravelling the *in vivo* consequences of GPR37/$A_{2A}R$ heteromer formation, the fingerprint for any named GPCR oligomer[33]. Thus, while we can't rule out existence of a heteromer-independent functional interplay, the following findings shed light regarding the *in vivo* function of the newly described striatal GPR37/$A_{2A}R$ heteromer: i) GPR37 and $A_{2A}R$

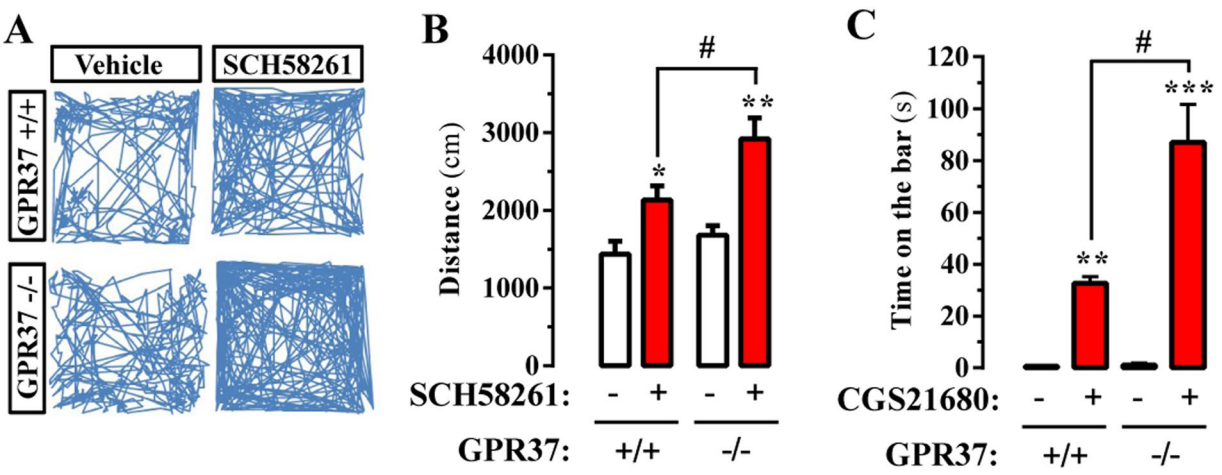

Figure 6. GPR37 deletion promotes $A_{2A}R$-mediated behavior. (**A**) $A_{2A}R$ antagonist-induced locomotor hyperactivity in GPR37+/+ and GPR37−/− mice. Representative 10 min trajectories in an open field arena of GPR37+/+ and GPR37−/− mice administered intraperitoneally with vehicle or SCH58261 (3.75 mg/kg). (**B**) Quantification of the horizontal locomotor activity shown in (**A**). The distance travelled is expressed as mean ± SEM (n = 10 animals) $^{*}P < 0.05$, $^{**}P < 0.01$ SCH58261 treatment effect (one-way ANOVA, followed by Tukey post-hoc test), $^{\#}P < 0.05$ phenotype effect (two-way ANOVA, Bonferroni post-hoc test). (**C**) $A_{2A}R$ agonist-induced catalepsy in GPR37+/+ and GPR37−/− mice. The cataleptic response induced by intracerebroventricular administration of CGS21680 (10 µl of a 1 µg/µl solution) in GPR37+/+ and GPR37−/− mice was measured as the duration of an abnormal upright posture in which the forepaws of the mouse were placed on a horizontal wooden bar. The time spent with both front paws resting on the bar is expressed as mean ± SEM (n = 10 animals); a cut off time was set at 200 s. $^{**}P < 0.01$, $^{***}P < 0.001$ CGS21680 treatment effect (one-way ANOVA, followed by Tukey post-hoc test); $^{\#}P < 0.05$ phenotype effect (Two-way ANOVA, Bonferroni post-hoc test).

displayed a high and selective anatomical proximity within striatal spines; ii) GPR37 deletion potentiated $A_{2A}R$ cell surface targeting in striatal slices; iii) $A_{2A}R$-mediated signaling was enhanced in striatal synaptosomes and primary cultures from GPR37−/−; iv) GPR37 deletion potentiated $A_{2A}R$ antagonist-mediated locomotor activity and $A_{2A}R$ agonist-induced catalepsy. Based on these data, we concluded that GPR37 is a negative modulator of $A_{2A}R$ cell surface expression and function *in vivo*, and whether the formation of the GPR37/$A_{2A}R$ heteromer is required for these effects should be further explored in the near future.

The striatum, the main input structure of the basal ganglia[34], is responsible for both movement and learning/reward behavior. Importantly, dopaminergic projections from the substantia nigra pars compacta (SNc) are essential for motor control and their degeneration in PD results in severe motor problems[35]. Indeed, conventional therapies for PD are primarily devoted to replacing and support dopaminergic neurotransmission. In such way, early PD motor symptoms respond well to dopamine-based therapies including levodopa and D_2R agonists[36]. However, in the long term, these agents may lead to the development of serious motor complications that limit their efficacy[37]. These therapeutic obstacles have prompted the search for alternative therapies based on novel nondopaminergic drug[38]. A new therapeutic target is the adenosinergic system. In fact, $A_{2A}R$ antagonists have not only been postulated but they have also been licensed as antiparkinsonian drugs[39]. Importantly, it is believed that the $A_{2A}R/D_2R$ heterodimer may underlie the observed antiparkinsonian effects of $A_{2A}R$ antagonists[40]. In addition, the striatal $A_{2A}R/D_2R$ heterodimer has been shown to be downregulated in experimental parkinsonism[19], a fact that parallels a concomitant increase in $A_{2A}R$ constitutive activity[28].

The ability of striatal GPR37 to oligomerize with $A_{2A}R$, and possibly with D_2R, might constitute a way for fine-tuning multiple receptor-signaling pathways and harmonizing dopaminergic neurotransmission. Certainly, manipulating the GPR37/$A_{2A}R$ heteromer stoichiometry could impact on D_2R functioning through putative postsynaptic GPR37/D_2R/$A_{2A}R$-containing complexes present in GABAergic striatopallidal neurons. Hence, it could be hypothesized that an increased GPR37/$A_{2A}R$ oligomerization would repress $A_{2A}R$ activity and, therefore, indirectly rise D_2R function, mimicking the effects of a direct activation of the receptor. This last hypothesis still needs to be experimentally probed, but it seems clear that the GPR37/$A_{2A}R$ heteromer, which here we demonstrate is formed in native conditions, may constitute a novel and very attractive target for the design of new pharmacological strategies to manage pathologies affecting dopaminergic neurotransmission such as PD.

Methods

Animals. C57BL/6J wild type (GPR37+/+) and GPR37 deficient (GPR37−/−) male mice (Strain Name: B6.129P2-*GPR37*^{tm1Dgen}/J; The Jackson Laboratory, Bar Harbor, ME, USA) with 8 weeks of age were used[2]. The University of Barcelona Committee on Animal Use and Care approved the protocol. Animals were housed and tested in compliance with the guidelines described in the Guide for the Care and Use of Laboratory Animals[41] and following the European Union directives (2010/63/EU). All efforts were made to minimize animal suffering and

the number of animals used. All animals were housed in groups of five in standard cages with *ad-libitum* access to food and water and maintained under 12 h dark/light cycle (starting at 7:30 AM), 22 °C temperature, and 66% humidity (standard conditions).

Immunohistoblotting. The regional distribution of GPR37 and $A_{2A}R$ was analyzed in the C57BL6 mouse brain using an *in situ* blotting technique[42,43]. Briefly, horizontal cryostat sections (25 μm) were placed on nitrocellulose membranes 0.45 μm (Whatman) moistened with 48 mM Tris-base, 39 mM glycine, 2% (w/v) SDS and 20% (v/v) methanol for 15 min at room temperature (~20 °C). After blocking in 5% (w/v) non-fat dry milk in phosphate-buffered saline, the nitrocellulose membranes were treated with Deoxyribonuclease I from bovine pancreas (DNase I, 5 U/mL, Sigma-Aldrich, St. Louis, MO, USA), washed and incubated in 2% (w/v) SDS and 100 mM β-mercaptoethanol in 100 mM Tris–HCl (pH 7.0) for 60 min at 45 °C to remove adhering tissue residues. After extensive washing, the blots were incubated overnight at 4 °C with rabbit anti-GPR37-N polyclonal antibody (3 μg/ml)[2] or goat anti-$A_{2A}R$ polyclonal antibody (AB_2571655; 3 μg/ml; Frontier Institute Co. Ltd, Shinko-nishi, Ishikari, Hokkaido, Japan) in blocking solution. The bound primary antibodies were detected with alkaline phosphatase-conjugated secondary antibodies. All nitrocellulose membranes were processed in parallel, using the same incubation times and antibody/reagent concentrations. Digital images were acquired with a Stereo Lumar.v12.

Fixed brain tissue preparation. Mice were anesthetized and perfused intracardially with 100 ml of ice-cold 4% paraformaldehyde (PFA) in phosphate buffered saline (PBS; 8.07 mM Na_2HPO_4, 1.47 mM KH_2PO_4, 137 mM NaCl, 0.27 mM KCl, pH 7.2). Brains were post-fixed overnight in the same solution of PFA at 4 °C. Coronal sections (50 μm) were obtained using a vibratome (Leica Lasertechnik GmbH, Heidelberg, Germany). Slices were collected in Walter's Antifreezing solution (30% glycerol, 30% ethylene glycol in PBS, pH 7.2) and kept at −20 °C until processing.

Immunoelectron microscopy. *Pre-embedding immunogold technique.* Immunohistochemical reactions for electron microscopy were carried out using the pre-embedding immunogold method described previously[44]. Briefly, free-floating sections were incubated in 10% (v/v) NGS (normal goat serum) diluted in TBS. Sections were then incubated with rabbit anti-GPR37-N (3–5 μg/ml diluted in TBS containing 1% (v/v) NGS), followed by incubation in goat anti-rabbit IgG coupled to 1.4 nm gold (Nanoprobes Inc., Stony Brook, NY, USA). Sections were post-fixed in 1% (v/v) glutaraldehyde and washed in double-distilled water, followed by silver enhancement of the gold particles with an HQ Silver kit (Nanoprobes Inc.). Sections were then treated with osmium tetraoxide (1% in 0.1 m phosphate buffer), block-stained with uranyl acetate, dehydrated in graded series of ethanol and flat-embedded on glass slides in Durcupan (Fluka, Sigma-Aldrich) resin. Regions of interest were cut at 70–90 nm on an ultramicrotome (Reichert Ultracut E, Leica, Austria) and collected on single slot pioloform-coated copper grids. Staining was performed on drops of 1% aqueous uranyl acetate followed by Reynolds's lead citrate. Ultrastructural analyses were performed in a Jeol-1010 electron microscope. To study the frequency of GPR37, we counted immunoparticles identified in each reference area and present in different subcellular compartments: dendritic spines, dendritic shafts and axon terminals. The data were expressed as a percentage of immunoparticles in each subcellular compartment, both in the plasma membrane and at intracellular sites.

Post-embedding immunogold technique. To study the spatial relationship between $A_{2A}R$ and GPR37 we used double-labelling post-embedding immunogold techniques, as previously described[45]. Briefly, ultrathin sections 80-nm thick from Lowicryl-embedded blocks of striatum were picked up on coated nickel grids and incubated on drops of a blocking solution consisting of 2% human serum albumin (HSA) in 0.05 M TBS and 0.03% Triton X-100 (TBST). The grids were incubated with a mixture of goat anti-$A_{2A}R$ and rabbit anti-GPR37-N (10 μg/ml in TBST with 2% HSA)[2] at 28 °C overnight. The grids were incubated on drops of rabbit anti-goat IgG or goat anti-rabbit IgG conjugated to 10 nm and 20 nm colloidal gold particles, respectively (BBI Solutions, Cardiff, UK) in 2% HSA and 0.5% polyethylene glycol in TBST. The grids were then washed in TBS and counterstained for electron microscopy with saturated aqueous uranyl acetate followed by lead citrate. Ultrastructural analyses were performed in a Jeol-1010 electron microscope. Randomly selected areas were then photographed from the selected ultrathin sections at a final magnification of 50,000 x.

Gel electrophoresis and immunoblotting. Sodium dodecyl sulfate–polyacrylamide gel electrophoresis (SDS/PAGE) was performed using 10% polyacrylamide gels. Proteins were transferred to polyvinylidene difluoride membranes using a semi-dry transfer system (Bio-Rad, Hercules, CA, USA) and immunoblotted using rabbit anti-GPR37-N (1 μg/ml)[2], goat anti-$A_{2A}R$ (AB_2571655; 1 μg/ml; Frontier Institute Co. Ltd), rabbit anti-synaptophysin (ab23754; 1 μg/ml; Abcam), mouse anti-PSD-95 (ab13552; 1 μg/ml; Abcam), mouse anti-SNAP-25 (ab66066; 1 μg/ml; Abcam) and rabbit anti-α-actinin (sc-15335; 0.5 μg/ml; Santa Cruz Biotechnology Inc., Dallas, TX, USA) antibodies. The primary antibodies were detected using a horseradish peroxidase (HRP)-conjugated goat anti-rabbit IgG (65–6120; 1/50,000; Pierce Biotechnology), HRP-conjugated goat anti-mouse IgG (31430; 1/20,000; Pierce Biotechnology), HRP-conjugated rabbit anti-goat IgG (61–1620; 1/20,000; Pierce Biotechnology). The immunoreactive bands were developed using a chemiluminescent detection kit (Thermo Fisher Scientific, Waltham, MA, USA) and detected with an Amersham Imager 600 (GE Healthcare Europe GmbH, Barcelona, Spain)[46].

Striatal slice biotinylation. Biotinylation is a useful tool for the covalent labelling and separation of cell-surface-expressed proteins in brain slices[47]. In brief, mouse brain was rapidly removed and immediately chilled in sucrose-supplemented artificial CSF (SACSF; 2.5 mM KCl, 1.2 mM NaH_2PO_4, 1.2 mM $MgCl_2$, 2.4 mM $CaCl_2$, 26 mM $NaHCO_3$, 11 mM glucose, and 250 mM sucrose) saturated with 95%O_2/5%CO_2. Brains were

mounted on a Leica vibratome 1200S sectioning system (Leica) and 300 µm coronal sections were made. Sections containing the striatum were recovered in ACSF (125 mM NaCl, 2.5 mM KCl, 1.2 mM NaH_2PO_4, 1.2 mM $MgCl_2$, 2.4 mM $CaCl_2$, 26 mM $NaHCO_3$, and 11 mM glucose) at 31 °C, during 90 min with 95% O_2/5% CO_2, then were immediately used. Surface proteins were covalently labeled with 0.5 mg/ml sulfo-NHS-SS-biotin in ice-cold ACSF for 45 min at 4 °C, with continuous 95%O_2/5%CO_2 bubbling. Following biotinylation, slices were washed 3 times in ice-cold ACSF and three times in ice-cold ACSF supplemented with 100 mM glycine. Residual reactive biotin was quenched by incubating twice in ice-cold ACSF supplemented with glycine during 25 min at 4 °C with continuous 95%O_2/5%CO_2 bubbling. Subsequently, slices were washed four times with ice-cold ACSF, triturated with iced-cold radio-immuno assay (RIPA) buffer (150 mM NaCl, 1% NP-40, 50 mM Tris, 0.5% sodium deoxycholate, and 0.1% SDS, pH 8.0) using a Pasteur pipette and rotated in an end over end rotator during 30 min at 4 °C. Cellular debris were cleared by centrifugation at 18,000 × *g* for 15 min at 4 °C and the protein concentration was determined using the bicinchoninic acid (BCA) protein assay (Pierce Biotechnology, Rockford, IL, USA). Next, 25 µl streptavidin agarose were added to 50 µg striatal lysate in 1 ml RIPA buffer and incubated overnight with constant rotation at 4 °C. Finally, streptavidin beads were washed five times with RIPA buffer and resuspended SDS-PAGE sample buffer for immunoblot assay. A rabbit anti-tyrosine hydroxylase antibody (AB152; Merck Millipore, Darmstadt, Germany) was used to ensure proper cell-surface-protein isolation.

Synaptosomal preparation and subsynaptic fractionation. For synaptosomal preparation the striatum from 6 mice were dissected and homogenized in 1 ml of isolation buffer (0.32 M sucrose, 0.1 mM $CaCl_2$ and 0.1 mM $MgCl_2$, pH 7.4) at 4 °C in a 5 ml Potter-Elvehjem glass tube using a homogenizer stirrer HS-30E (Witeg Labortechnik GmbH, Wertheim, Germany) with 10 *strokes* at 700–900 rotations per min. The resulting homogenate was mixed with 6 ml sucrose 2 M and 2.5 mL $CaCl_2$ 0.1 mM in an ultra-clear centrifuge tube (Beckman Coulter, Hospitalet de Llobregat, Spain). Then, 2.5 mL of sucrose 1 M containing 0.1 mM $CaCl_2$ were slowly added on top of the tube to form a sucrose gradient. After centrifugation for 3 h at 100,000 x *g* at 4 °C, the synaptosomes were collected as the interphase between 1.25 M and 1 M sucrose. They were diluted 10 times in isolation buffer, centrifuged for 30 min at 15,000 × *g* at 4 °C and the resulting synaptosomal pellet was resuspended in 1 ml of isolation buffer for immediate use.

The separation of the presynaptic active zone, postsynaptic density and extrasynaptic fractions from striatal synapses was carried out as previously described[48]. Briefly, synaptosomes were diluted 1:10 in cold 0.1 mM $CaCl_2$ and an equal volume of 2 x solubilization buffer (2% Triton X-100, 40 mM Tris, pH 6.0) was added to the suspension. The suspension was incubated for 30 min on ice with constant agitation and the insoluble material (synaptic junctions) pelleted (40,000 × *g* for 30 min at 4 °C). The supernatant (extrasynaptic fraction) was concentrated using an Amicon Ultra 15 10K (Merck Millipore) and proteins precipitated with six volumes acetone at −20 °C and recovered by centrifugation (18,000 × *g* for 30 min at −15 °C). The synaptic junctions pellet was washed in solubilization buffer (pH 6.0) and resuspended in 10 volumes of a second solubilization buffer (1% Triton X-100, 20 mM Tris at pH 8.0). After incubation for 30 min on ice with agitation, the mixture was centrifuged and the supernatant (presynaptic fraction) processed as described for the extrasynaptic fraction, whereas the insoluble pellet corresponds to the postsynaptic fraction. Protease inhibitors (Protease Inhibitor Cocktail Set III, Millipore, Temecula, CA, USA) were added to the suspension in all extraction steps. The protein concentration was determined by the BCA protein assay (Pierce Biotechnology) and 20 ug of each fraction, solubilized in 5% SDS, were added to SDS-PAGE sample buffer prior to freezing at −20 °C.

cAMP assay in synaptosomes. Synaptosomal cAMP accumulation was measured using the LANCE Ultra cAMP kit (PerkinElmer, Waltham, MA, USA) as previously described[49]. In brief, total striatal synaptosomal membranes (0.5 µg) from GPR37+/+ and GPR37−/− mice were resuspended in stimulation buffer (HBSS 1X, 5 mM Hepes pH 7.4, 10 mM $MgCl_2$, 0.1% BSA) and subsequently processed for cAMP accumulation. Thus, vehicle, forskolin (1 µM; Sigma-Aldrich) or CGS21680 (500 nM; Tocris Biosciences, Bristol, UK) were added for 30 min at 22 °C before the lysis and cAMP quantification in a POLARStar microplate reader (BMG Labtech, Durham, NC, USA). cAMP levels were calculated as previously described[49].

Striatal primary cell culture. Primary striatal neurons were cultured from GPR37+/+ and GPR37−/− mice embryos (E18). Briefly, after dissection, the striatum was treated with 1.25% trypsin for 10 min (Sigma-Aldrich) and mechanically dissociated with a flame polished Pasteur pipette. Neurons were plated onto poly-D-lysine (0.1 mg/ml) and laminin-coated (0.01 mg/ml) 6-wells plate (for cAMP accumulation assay) or 12-wells plate containing glass coverslips (for immunocytochemistry) in minimum essential medium (Invitrogen, Carlsbad, CA, USA) supplemented with 10% horse serum, 10% bovine serum, 1 mM pyruvic acid, and 0.59% glucose at a density of 80,000 cells/cm^2. After 4–14 h, the medium was substituted with Neurobasal medium supplemented with penicillin (100 U/ml), streptomycin (100 µg/ml), 0.59% glucose, and B27 supplement (Invitrogen). Neurons were kept at 5% CO_2, 37 °C and 95% humidity for 21 days *in vitro* (DIV) before the experiments.

Immunofluorescence. For immunohistochemistry of brain slices, these were washed three times with PBS, permeabilized with 0.5% Triton X-100 in PBS for 2 hours and rinsed again three times with washing solution (0.05% Triton X-100 in PBS). The slices were then incubated with washing solution containing 10% normal donkey serum (NDS; Jackson ImmunoResearch Laboratories, Inc., West Grove, PA, USA) for 2 h at room temperature. Subsequently, slices were incubated with a new homemade rabbit anti-GPR37 polyclonal antibody, raised using a glutathione S-transferase (GST)-fusion protein containing amino acids 541–600 of GPR37 C terminus (anti-GPR37-C: 3 µg/ml), plus goat anti-A_{2A}R (3 µg/ml; Frontier Institute Co. Ltd) in washing solution containing 10% NDS for 48h at 4 °C. Next, slices were washed with washing solution containing 1% NDS before the incubation with Cy3-conjugated donkey anti-rabbit IgG antibody (1/200; Jackson ImmunoResearch Laboratories) and

Cy2-conjugated donkey anti-goat IgG antibody (1/200; Jackson ImmunoResearch Laboratories) in washing solution for 2 h at room temperature. Finally, slices were washed twice with 1% NDS in washing solution containing 10% NDS and then mounted with Vectashield immunofluorescence medium (Vector Laboratories, Peterborough, UK) in glass slides. Fluorescence striatal images were captured using a Leica TCS 4D confocal scanning laser microscope (Leica Lasertechnik GmbH).

For immunocytochemistry of DIV21 primary striatal neurons, these were grown on poly-D-lysine (0.1 mg/ml) and laminin-coated (0.01 mg/ml) coverslips, fixed in 4% paraformaldehyde for 15 min and washed with PBS containing 20 mM glycine (buffer A) to quench aldehyde groups. Neurons were then permeabilized with buffer A containing 0.2% Triton X-100 for 10 min. Subsequently, neurons were labeled for 1 h at 22 °C with a rabbit anti-GPR37-N antibody (1 μg/ml) and a goat anti-$A_{2A}R$ (1 μg/ml) washed, and stained with Cy5-conjugated donkey anti-rabbit IgG antibody (1/200) and Cy2-conjugated donkey anti-goat IgG antibody (1/200) (Jackson ImmunoReserach Laboratories Inc.). Coverslips were rinsed for 3 min in PBS, mounted with Vectashield immunofluorescence medium (Vector Laboratories) and examined using a Leica TCS 4D confocal scanning laser microscope (Leica Lasertechnik GmbH, Heidelberg, Germany).

For immunostaining of synaptosomes, total synaptosomes from striatum were fixed in 4% paraformaldehyde for 15 min using an end over end tube rotator at room temperature. Subsequently, 100 μl of a 0.125 mg/ml synaptosomal suspension was platted onto poly-D-lysine (0.1 mg/ml)-coated coverslips for 1 hour at 37 °C in a humidity chamber. Next, coverslips were processed as described for immunocytochemistry experiments with cultured neurons. Each coverslip was analysed by counting three different fields.

Proximity ligation *in situ* assay. Duolink *in situ* PLA detection Kit (Olink Bioscience, Uppsala, Sweden) was performed in a similar manner as immunohistochemistry using rabbit anti-GPR37-C (3 μg/ml) plus goat anti-$A_{2A}R$ (3 μg/m) as a primary antibodies and the secondary antibodies following the manufacturer's protocol, as previously described[19,26]. Fluorescence images were acquired on a Leica TCS 4D confocal scanning laser microscope (Leica Lasertechnik GmbH) using a 60x N.A. = 1.42 oil objective from the selected area. High-resolution images were acquired as a z-stack with a 0.2 μm z-interval with a total thick of 5 μm. Nonspecific nuclear signal was eliminated from PLA images by substracting TO-PRO-3 Iodide (Thermo Fisher Scientific) labeling. Analyze particle function from Image J (NIH) was used to count particles larger than 0.3 μm^2 for PLA signal and larger than 100 μm^2 to discriminate neuronal from glia nuclei[50]. For each image several oligomer particles and neuron nuclei was obtained and ratio among them was calculated.

Striatal primary cell culture cAMP assay. For cAMP assay, mouse striatal neurons were grown on a 6-wells plate. On DIV21, cAMP accumulation was measured using the cAMP HiRange assay Kit (CisBio, Bagnols-sur-Cèze, France). The growing media of striatal neurons was replaced by non-supplemented Neurobasal with adenosine deaminase (ADA, 5 μg/well; from Roche Diagnostics GmbH, Mannheim, Germany) and incubated for 2h. Subsequently, zardaverine (50 μM; Tocris Bioscience) was added and incubated for 30 min at 37 °C. Next, vehicle, forskolin (1 μM; Sigma-Aldrich) or CGS21680 (500 nM; Tocris Biosciences) were added for 30 min at 37 °C before the lysis with 250 μl of lysis buffer (CisBio). The neuronal extract was centrifuged at 13,000 × *g* for 30 min at 4 °C. The cAMP content in 10 μl of the supernatant was determined as previously described[49].

Catalepsy induction test. Catalepsy was induced in mice by the intracerebroventricular (i.c.v.) administration of CGS21680 (10 μg), as previously described[51]. The cataleptic response was measured as the duration of an abnormal upright posture in which the forepaws of the mouse were placed on a horizontal wooden bar (0.6 cm of diameter) that was located 4.5 cm above the floor. The latency to move at least one of the two forepaws was recorded 2h after CGS21680 administration.

Open-field test. To evaluate the spontaneous locomotor activity, we performed the open field test. In brief, the mice were placed in the center of an activity field arena (30 × 30 cm, surrounded by four 50 cm high black painted walls) equipped with a camera above to record activity. Mice were administered (ip) with vehicle or SCH58261 (3.75 mg/kg; Abcam Biochemicals, Cambridge, UK) 15 min before measuring the exploratory behavior of the animals during a 10-min period. The total distance travelled and the activity within the outer and inner zone of the open field was analyzed using Spot tracker function from Image J (NIH). All behavioral tests were carried out in a sound attenuated room with 15 lux illumination. The apparatus and the objects were cleaned with a 70% alcohol solution and rinsed with water after each session.

Statistics. The number of samples (n) in each set of experimental conditions is indicated in figure legends. Statistical analysis was performed by one-way ANOVA followed by Tukey *post-hoc* test, two-way ANOVA followed by Bonferroni *post-hoc* test or Student's *t*-test when appropriate. Statistical significance was considered at $P < 0.05$.

References

1. Donohue, P. J. *et al.* A human gene encodes a putative G protein-coupled receptor highly expressed in the central nervous system. *Brain research. Molecular brain research* **54**, 152–60 (1998).
2. Lopes, J. P. *et al.* The role of parkinson's disease-associated receptor GPR37 in the hippocampus: functional interplay with the adenosinergic system. *Journal of Neurochemistry* **134**, 135–146 (2015).
3. Berger, B. S., Acebron, S. P., Herbst, J., Koch, S. & Niehrs, C. Parkinson's disease?associated receptor GPR37 is an ER chaperone for LRP6. *EMBO reports* **18**, 712–725 (2017).
4. Yang, H.-J., Vainshtein, A., Maik-Rachline, G. & Peles, E. G protein-coupled receptor 37 is a negative regulator of oligodendrocyte differentiation and myelination. *Nature communications* **7**, 10884 (2016).
5. Imai, Y. *et al.* An unfolded putative transmembrane polypeptide, which can lead to endoplasmic reticulum stress, is a substrate of Parkin. *Cell* **105**, 891–902 (2001).

6. Kitada, T. *et al*. Mutations in the parkin gene cause autosomal recessive juvenile parkinsonism. *Nature* **392**, 605–8 (1998).
7. Shimura, H. *et al*. Familial Parkinson disease gene product, parkin, is a ubiquitin-protein ligase. *Nature genetics* **25**, 302–305 (2000).
8. Sriram, S. R. *et al*. Familial-associated mutations differentially disrupt the solubility, localization, binding and ubiquitination properties of parkin. *Human molecular genetics* **14**, 2571–2586 (2005).
9. Mattila, S. O., Tuusa, J. T. & Petäjä-Repo, U. E. The Parkinson's-disease-associated receptor GPR37 undergoes metalloproteinase-mediated N-terminal cleavage and ectodomain shedding. *Journal of cell science* **129**, 1366–77 (2016).
10. Meyer, R. C., Giddens, M. M., Schaefer, S. A. & Hall, R. A. GPR37 and GPR37L1 are receptors for the neuroprotective and glioprotective factors prosaptide and prosaposin. *Proceedings of the National Academy of Sciences of the United States of America* **110**, 9529–34 (2013).
11. Murakami, T. *et al*. Pael-R is accumulated in Lewy bodies of Parkinson's disease. *Annals of Neurology* **55**, 439–442 (2004).
12. Yang, Y., Nishimura, I., Imai, Y., Takahashi, R. & Lu, B. Parkin suppresses dopaminergic neuron-selective neurotoxicity induced by Pael-R in Drosophila. *Neuron* **37**, 911–924 (2003).
13. Kitao, Y. *et al*. Pael receptor induces death of dopaminergic neurons in the substantia nigra via endoplasmic reticulum stress and dopamine toxicity, which is enhanced under condition of parkin inactivation. *Human molecular genetics* **16**, 50–60 (2007).
14. Imai, Y. *et al*. Pael receptor is involved in dopamine metabolism in the nigrostriatal system. *Neuroscience research* **59**, 413–25 (2007).
15. Marazziti, D. *et al*. GPR37 associates with the dopamine transporter to modulate dopamine uptake and behavioral responses to dopaminergic drugs. *Proceedings of the National Academy of Sciences of the United States of America* **104**, 9846–9851 (2007).
16. Gandía, J., Morató, X., Stagljar, I., Fernández-Dueñas, V. & Ciruela, F. Adenosine A2A receptor-mediated control of pilocarpine-induced tremulous jaw movements is Parkinson's disease-associated GPR37 receptor-dependent. *Behavioural brain research* **288**, 103–6 (2015).
17. Dunham, J. H., Meyer, R. C., Garcia, E. L. & Hall, R. A. GPR37 surface expression enhancement via N-terminal truncation or protein-protein interactions. *Biochemistry* **48**, 10286–10297 (2009).
18. Sokolina, K. *et al*. Systematic protein–protein interaction mapping for clinically relevant human GPCRs. *Molecular Systems Biology* **13**, 918 (2017).
19. Fernández-Dueñas, V. *et al*. Untangling dopamine-adenosine receptor-receptor assembly in experimental parkinsonism in rats. *Disease Models & Mechanisms* **8**, 57–63 (2015).
20. Borrelli, E. *et al*. Distinct functions of the two isoforms of dopamine D2 receptors. *Nature* **408**, 199–203 (2000).
21. Rosin, D. L., Hettinger, B. D., Lee, A. & Linden, J. Anatomy of adenosine A2A receptors in brain: morphological substrates for integration of striatal function. *Neurology* **61**, S12–8 (2003).
22. Rosin, D. L., Robeva, A., Woodard, R. L., Guyenet, P. G. & Linden, J. Immunohistochemical localization of adenosine A2A receptors in the rat central nervous system. *The Journal of comparative neurology* **401**, 163–186 (1998).
23. Rebola, N., Canas, P. M., Oliveira, C. R. & Cunha, R. A. Different synaptic and subsynaptic localization of adenosine A2A receptors in the hippocampus and striatum of the rat. *Neuroscience* **132**, 893–903 (2005).
24. Morató, X., López-Cano, M., Canas, P. M., Cunha, R. A. & Ciruela, F. Brain Membrane Fractionation: An *Ex Vivo* Approach to Assess Subsynaptic Protein Localization. *Journal of Visualized Experiments*. doi:10.3791/55661 (2017).
25. Fuxe, K. *et al*. Extrasynaptic Neurotransmission in the Modulation of Brain Function. Focus on the Striatal Neuronal–Glial Networks. *Frontiers in Physiology* **3**, 136 (2012).
26. Taura, J., Fernández-Dueñas, V. & Ciruela, F. Visualizing G Protein-Coupled Receptor-Receptor Interactions in Brain Using Proximity Ligation *In Situ* Assay. *Current protocols in cell biology/editorial board, Juan S. Bonifacino… [et al.]* **67**, 17.17.1–17.17.16 (2015).
27. Fuxe, K. *et al*. Receptor heteromerization in adenosine A2A receptor signaling: relevance for striatal function and Parkinson's disease. *Neurology* **61**, S19–23 (2003).
28. Fernández-Dueñas, V. *et al*. Uncovering Caffeine's Adenosine A2A Receptor Inverse Agonism in Experimental Parkinsonism. *ACS chemical biology* **9**, 2496–501 (2014).
29. Ferré, S. Adenosine-dopamine interactions in the ventral striatum. *Implications for the treatment of schizophrenia. Psychopharmacology* **133**, 107–20 (1997).
30. Cabeza de Vaca, S. *et al*. The adenosine A2A receptor agonist, CGS-21680, blocks excessive rearing, acquisition of wheel running, and increases nucleus accumbens CREB phosphorylation in chronically food-restricted rats. *Brain Research* **1142** 100–109 (2007).
31. Hauber, W. & Münkle, M. Motor depressant effects mediated by dopamine D2 and adenosine A2A receptors in the nucleus accumbens and the caudate-putamen. *European Journal of Pharmacology* **323**, 127–31 (1997).
32. Wardas, J., Konieczny, J. & Pietraszek, M. Influence of CGS-21680, a selective adenosine A2A agonist, on the phencyclidine-induced sensorimotor gating deficit and motor behaviour in rats. *Psychopharmacology* **168**, 299–306 (2003).
33. Ciruela, F. *et al*. G protein-coupled receptor oligomerization for what? *Journal of receptor and signal transduction research* **30**, 322–330 (2010).
34. Albin, R. L., Young, A. B. & Penney, J. B. The functional anatomy of disorders of the basal ganglia. *Trends in neurosciences* **18**, 63–4 (1995).
35. Dauer, W. & Przedborski, S. Parkinson's disease: mechanisms and models. *Neuron* **39**, 889–909 (2003).
36. Romrell, J., Fernandez, H. H. & Okun, M. S. Rationale for current therapies in Parkinson's disease. *Expert opinion on pharmacotherapy* **4**, 1747–61 (2003).
37. Huot, P., Johnston, T. H., Koprich, J. B., Fox, S. H. & Brotchie, J. M. The pharmacology of L-DOPA-induced dyskinesia in Parkinson's disease. *Pharmacological reviews* **65**, 171–222 (2013).
38. Kalia, L. V., Brotchie, J. M. & Fox, S. H. Novel nondopaminergic targets for motor features of Parkinson's disease: review of recent trials. *Movement disorders: official journal of the Movement Disorder Society* **28**, 131–44 (2013).
39. Jenner, P. Istradefylline, a novel adenosine A2A receptor antagonist, for the treatment of Parkinson's disease. *Expert opinion on investigational drugs* **14**, 729–738 (2005).
40. Ferré, S., Fuxe, K., B. Fredholm, B., Morelli, M. & Popoli, P. Adenosine–dopamine receptor–receptor interactions as an integrative mechanism in the basal ganglia. *Trends in Neurosciences* **20**, 482–487 (1997).
41. Clark, J. D., Gebhart, G. F., Gonder, J. C., Keeling, M. E. & Kohn, D. F. Special Report: The 1996 Guide for the Care and Use of Laboratory Animals. *ILAR journal/National Research Council, Institute of Laboratory Animal Resources* **38**, 41–48 (1997).
42. Tonnes, J. *et al*. Regional distribution and developmental changes of GluR1-flop protein revealed by monoclonal antibody in rat brain. *Journal of neurochemistry* **73**, 2195–2205 (1999).
43. Fernández-Alacid, L., Watanabe, M., Molnár, E., Wickman, K. & Luján, R. Developmental regulation of G protein-gated inwardly-rectifying K+ (GIRK/Kir3) channel subunits in the brain. *The European journal of neuroscience* **34**, 1724–36 (2011).
44. Lujan, R., Nusser, Z., Roberts, J. D., Shigemoto, R. & Somogyi, P. Perisynaptic location of metabotropic glutamate receptors mGluR1 and mGluR5 on dendrites and dendritic spines in the rat hippocampus. *The European journal of neuroscience* **8**, 1488–1500 (1996).
45. Lujan, R. *et al*. Immunocytochemical localization of metabotropic glutamate receptor type 1 alpha and tubulin in rat brain. *Neuroreport* **12**, 1285–1291 (2001).
46. Morató, X., Borroto-Escuela, D. O., Fuxe, K., Fernández-Dueñas, V. & Ciruela, F. Co-immunoprecipitation from brain. *Neuromethods* **110**, 19–30 (2016).
47. Gladding, C. M. *et al*. Tyrosine dephosphorylation regulates AMPAR internalisation in mGluR-LTD. *Molecular and cellular neurosciences* **40**, 267–79 (2009).

48. Phillips, G. R. *et al*. The presynaptic particle web: ultrastructure, composition, dissolution, and reconstitution. *Neuron* **32**, 63–77 (2001).
49. Taura, J., Fernández-Dueñas, V. & Ciruela, F. Determination of GPCR-mediated cAMP accumulation in rat striatal synaptosomes. *Neuromethods* **110**, 455–464 (2016).
50. Matamales, M. *et al*. Striatal medium-sized spiny neurons: identification by nuclear staining and study of neuronal subpopulations in BAC transgenic mice. *PLoS One* **4**, e4770 (2009).
51. Khisti, R. T., Chopde, C. T. & Abraham, E. GABAergic involvement in motor effects of an adenosine A(2A) receptor agonist in mice. *Neuropharmacology* **39**, 1004–1015 (2000).

Acknowledgements

This work was supported by MINECO/ISCIII (SAF2014–55700-P and PIE14/00034), the Catalan government (2014 SGR 1054), Fundació la Marató de TV3 (Grant 20152031) and FWO (SBO-140028) to FC and Santa Casa da Misericórdia to RAC. Also supported by MINECO (BFU-2015-63769-R), Junta de Comunidades de Castilla-La Mancha (PPII-2014-005-P) and European Union (HBP - Project Ref. 604102) to R.L. We thank Esther Castaño and Benjamín Torrejón, from the CCiT-Bellvitge Campus of the University of Barcelona for the technical assistance.

Author Contributions

X.M. performed in cell and *in vivo* experiments and analysed animal behaviour. R.L. immunogold experiments and wrote the paper. M.L-C. performed in cell experiments and analysed the data. J.G. performed in cell experiments. I.S. analysed data and wrote the paper. M.-W. analysed data and wrote the paper. R.A.C. analysed data and wrote the paper. V.F-D. analysed data and wrote the paper. F.C. conceived and supervised the project, designed experiments, analysed data and wrote the paper.

Additional Information

Competing Interests: The authors declare that they have no competing interests.

Publisher's note: Springer Nature remains neutral with regard to jurisdictional claims in published maps and institutional affiliations.